Journal of Non-Crystalline Solids 354 (2008) 1721–1730

New large grain, highly crystalline, transparent glass–ceramics

Thiana Berthier [a], Vladimir M. Fokin [b], Edgar D. Zanotto [a,*]

[a] *Vitreous Materials Laboratory, Department of Materials Engineering, Federal University of São Carlos, 13.565-905 São Carlos, SP, Brazil*
[b] *S.I. Vavilov State Optical Institute, ul. Babushkina 36/1, St. Petersburg 192131, Russia*

Received 28 November 2006; received in revised form 13 August 2007
Available online 1 October 2007

Abstract

Two main reasons assure the transparency in the visible of some glass–ceramics (TGC): their crystal sizes are much smaller than the wavelength of light or the difference between the refractive index of glass matrix and crystal phase is small. The majority of traditional TGC have nano-size crystals and small to moderate crystallized volume fraction, usually between 3% and 70%. In this article we present a new type of transparent glass–ceramics having large (micrometric) grain size and very high crystallized volume fraction, which reaches up to 97%. Their high transparency mainly results from simultaneous variations of the glass matrix and crystal compositions during crystallization, which considerably decreases the difference between the respective refractive indexes, and this factor prevails, regardless of crystal size. Preliminary tests of their optical properties indicate that this new family of TGC can be further developed by doping with transition metals and rare-earths.

PACS: 61.43.Fs; 64.70.dj; 64.60.Q

Keywords: Crystallization; Crystal growth; Glass ceramics; Nucleation; Oxide glasses; Alkali silicates; Silicates; Soda-lime–silica

1. Introduction

Glass–ceramic technology is based on controlled crystal nucleation and growth in certain glasses, and has several advantages over conventional powder-processed ceramics, such as very low or null porosity, as well as uniformity and reproducibility of microstructure. The crystalline phases precipitated in some glass matrices typically enhance and sometimes lead to entirely new combination of properties. Some of the technologically most important glass–ceramics have, for instance, low thermal expansion coefficients coupled with high thermal and chemical stability, high mechanical strength and optical transparency [1].

Recently, much attention has been devoted to optically transparent glass–ceramics that have improved optical properties, greater thermal stability and strength than their parent glasses [2,3]. Dozens of papers and patents on transparent glass–ceramics have been registered worldwide in the last thirty years (see, e.g. [4]). Applications of these transparent crystalline materials, which are capable of being shaped by fast and flexible glass-forming processes, are numerous and include cooking ware, fire resistant plates, security windows, hosting medium for transition metals and rare-earths among others [5].

This paper focuses on the development and characterization of a new type of transparent glass–ceramic. The originality of this material is based on a tight control of homogeneous nucleation and growth of solid solution crystals with a continuous variation of the compositions of both crystalline and glassy phases during phase transformation. This unique evolution reduces the difference between the refractive indexes of crystals and residual glass. The crystallinity of this new TGC can reach up to 97% (spontaneous cracking takes place for higher crystallinities) with grain sizes of about 5–7 μm, in contrast to conventional TGC that have nano-metric microstructures

* Corresponding author. Tel.: +55 16 3351 8527; fax: +55 16 3361 5404.
E-mail address: dedz@power.ufscar.br (E.D. Zanotto).
URL: www.lamav.ufscar.br (E.D. Zanotto).

0022-3093/$ - see front matter
doi:10.1016/j.jnoncrysol.2007.08.052

and low to moderate crystallized volume fraction. Some of the characteristic optical properties of these new, large grain transparent glass–ceramics are presented below together with an analysis of their crystallization process.

2. Brief literature review

Some of the most important proposed applications of TGC refer to optical components and devices including: laser media; saturable absorber media; illumination devices using infrared light; heat-resistant materials that absorb ultraviolet light, TGCs that reflect infrared light and are transparent to visible light; substrates for arrayed waveguide grating (AWG) [6,7]; radiation sources of lamps; laser pumps; substrate materials; wafer stages; mirror support for telescopes; second harmonic generation (optical energy converting elements) [8,9]; front windows in heating furnaces or slow-cooling reactors; precise photolithography; blue or green state lasers, LCD substrates, optical amplifiers for wavelength up-conversion [10]; ring laser gyroscopes; materials that absorb UV and fluoresce in the red/IR (possibly used as tunable lasers) [11]; solar collectors; printed optical circuits; gradient refraction optical lenses; optical waveguides [12–14], etc.

There are several patents on transparent glass–ceramics that contain a major crystalline phase of low thermal expansion coefficient (0.1×10^{-6}–1.0×10^{-6}/K) and thus present high thermal shock resistance [4]. Transparency is usually observed in glass–ceramics containing relatively small to moderate volume fractions of crystals (3–70%) with nanoscale size (1–15 nm) [15]. The majority of these low expansion materials belong to the lithia–alumina–silica family with titanium and/or zirconia as nucleating agents, and a number of minor elements to impart color or to improve processability, and have beta-quartz solid solution as the major phase [16].

3. Theoretical background

There are two distinct ways in which light intensity can be attenuated by a medium: atomic absorption and scattering [17,18]. A combination between these two mechanisms plus light reflection from the external surfaces can be expressed by the following equation:

$$I = I_0(1-R)^2\exp[-(\beta+S)x], \tag{1}$$

where

$$R = \left(\frac{n-1}{n+1}\right)^2,$$

and I_0 and I are the initial and transmitted light intensity, respectively, β the linear absorption coefficient (absorption index), S the scattering coefficient, x the optical path length, and n is the refractive index of the TGC.

The scattering coefficient S can be written as

$$S = K\pi r^2 N, \tag{2}$$

or assuming spherical particles, as

$$S = \frac{3}{4}KVr^{-1}, \tag{3}$$

where N and V are the number density and volume fraction of the scattering particles, respectively, and K is a scattering factor.

K increases with particle-size, reaches a maximum when the particle-size is close to λ, and decreases for larger particle-sizes, approaching a constant value for $r \gg \lambda$. Thus, according to Eq. (3), for a fixed concentration (V) of scattering phase the measured scattering coefficient decreases with increasing particle-size (see, e.g. [19]).

If a scattering medium has particles with sizes less than 0.1–0.2 of the typical wavelength of visible light, Rayleigh scattering takes place and the angular distribution of scattered light can be written as [3]

$$I = \frac{(1+\cos^2\theta)}{L^2}\frac{8\pi^4}{\lambda^4}r^6\left[\frac{M^2-1}{M^2+2}\right]^2 I_0, \tag{4}$$

where θ is the scattering angle, L is the distance from the scattering centers of radius r, and M is the ratio of the refractive index of the particle to that of the surrounding medium. According to Eq. (4) the scattered intensity depends mainly on the ratio of the particle-size to the wavelength of light, r/λ, and the ratio of refractive indexes, M. Thus, for any given value of θ, L, and λ, the smaller the first ratio and the closer to unity the second, the most transmitting is the medium.

If the sizes of the scattering centers are comparable or larger than the wavelength of visible light (as in the case of the micrometric crystals of our TGC), the simple Rayleigh theory breaks down. For such relatively large crystal sizes, the dependence of the scattered light intensity on λ becomes weaker than that for the Rayleigh scattering, and is given by

$$I \sim \lambda^{-p}, \tag{5}$$

where $p < 4$ and decreases with increasing particle-size. Due to the interference of light scattered by different parts of each scattering particle, the $I(\theta)$ dependence becomes more complicated. With increasing particles sizes forward scattering (acute angles) prevails back scattering (obtuse angles), the so-called Mie effect. This effect may lead to a decrease of the measured scattering coefficient (contrary to the case of small particles) with increasing particle-sizes.

4. Materials and experimental procedures

Sodium and calcium carbonates, and crushed quartz were used as starting materials. After melting the proper mixtures in a platinum crucible at 1300–1500 °C for about 4 h, the melts were cast on massive metallic plates to give about 5 mm thick specimens. The compositions of the glasses were close to the pseudo-binary join $CaO\cdot SiO_2$–$Na_2O\cdot SiO_2$ in the interval ($Na_2O\cdot 2CaO\cdot 3SiO_2$($N_1C_2S_3$)–$Na_2O\cdot CaO\cdot 2SiO_2$($N_1C_1S_2$)) of solid solution formation. Table 1 shows typical compositions of the TGCs here investigated.

Table 1
Examples of some our TGC compositions in mol%

TGC	SiO_2	Na_2O	CaO
TGC-0[a]	50.2	19.2	30.6
TGC-1[b]	49.0	18.8	32.3
TGC-2[a]	50.0	16.7	33.1

[a] By analysis.
[b] This TGC was doped with 0.2 and 0.5 wt% Er.

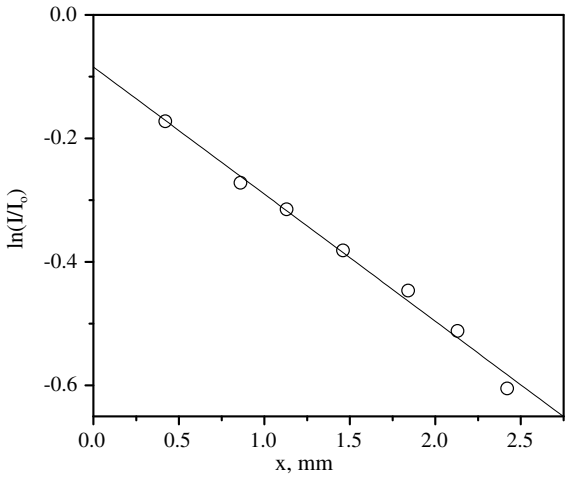

Fig. 1. $\ln(I/I_0)$ versus x typical plot for TGC-0 with about 3% of crystallinity fitted by a linear function.

The degree of crystallinity and crystal sizes were measured by optical microscopy with a pattern analyzer. The crystal and glassy matrix compositions were estimated via energy dispersive spectroscopy (EDS) using Stereoscan 440 Link/Oxford. The excitation volume of the electron beam was about 2–3 μm in diameter. The parent glass and a fully crystallized glass were employed as standards. About six measurements were performed for both glassy and crystalline phases to evaluate the average values.

Spectra of the partly and fully crystallized glasses, shaped as parallel-sided polished plates, were recorded in the range of 200–1100 nm to characterize their transmittance as a function of crystallinity. To estimate the parameters $P_1 = (1-R)^2$ and $P_2 = (\beta + S)$ of Eq. (1) characterizing the energy loss due to light reflection, absorption and scattering, respectively, the transmittance I/I_0 was measured as a function of sample thickness, x. Fig. 1 shows a $\ln(I/I_0)$ versus x plot approximated by a linear function $Y = A - Bx$ where $A = \ln(P_1)$ and $B = P_2$.

The refractive indexes of the parent glasses and TGCs were measured with an Abbe refractometer using the NaD line ($\lambda = 589$ nm). The Abbe numbers (υ_d) were calculated by the following equation

$$\upsilon_d = \frac{(n_d - 1)}{(n_f - n_c)}, \tag{6}$$

where n_d, n_f, and n_c are the refractive index at $\lambda = 589$, 486, and 643 nm, respectively [20].

A Netzsch DSC 404 equipment was employed for the determination of the characteristic temperatures in the heating and cooling curves using bulk samples of about 20–30 mg.

5. Results

The crystals grown in the present glasses are solid solutions (s/s) having the chemical formula $Na_{4+2x}Ca_{4-x}[Si_6O_{18}]$ $(0 \leqslant x \leqslant 1)$. These s/s are formed by replacement of 1Ca by 2Na [21–23].

At a temperature T_{pm}, well below the glass transition temperature, T_g, the solid solutions with $0 < x < 0.5$ reveal a reversible polymorphic transition, which is accompanied by a clear thermal effect in the DSC curves (Fig. 2) also reported in Ref. [24]. The value of T_{pm} strongly decreases with decreasing sodium content (see Fig. 3) and thus can be employed to characterize the crystal composition, see Ref. [25].

Depending on the parent glass composition, the crystals are approximately spheric or cubic shaped, such as those shown in Fig. 4. Crystals with mixed shapes were occasionally observed as has been already noted in Ref. [26]. Excess of SiO_2 relative to the metasilicate composition favors spherical crystals, while a deficit in SiO_2 favors the formation of cubic shaped crystals.

Fig. 5 shows the XRD patterns of almost fully crystallized samples TGC1 and TGC2 with crystals of cubic and spherical morphologies, respectively. Both morphologies refer to solid solutions based on the hexagonal structure

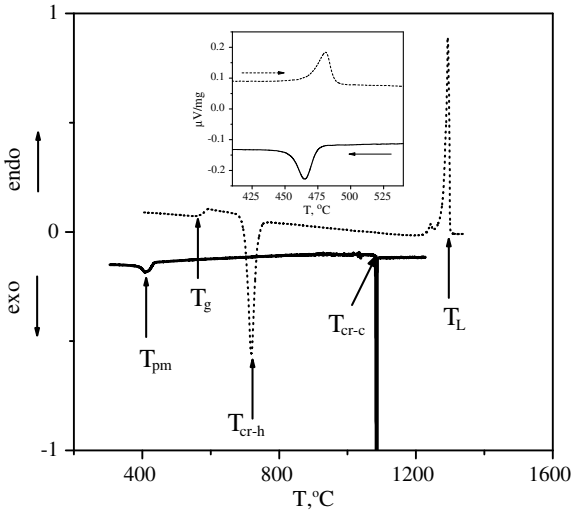

Fig. 2. Typical DSC heating and cooling curves for glass TGC-0. The dotted and solid lines refer to heating and cooling with rates ±10 K/min, respectively. Arrows denote the characteristic temperatures: glass transition, T_g, crystallization during heating, $T_{cr\text{-}h}$, and cooling, $T_{cr\text{-}c}$, liquidus, T_L, and the reversible phase transition, T_{pm}. The 'pre-melting' peak is likely caused by the peculiarities of the s/s melting between solidus and liquidus. It should be noted that this peak is typical for compositions that are shifted relative to stoichiometric composition $N_1C_2S_3$. The inset shows DSC heating and cooling curves for a fully crystallized TGC-2.

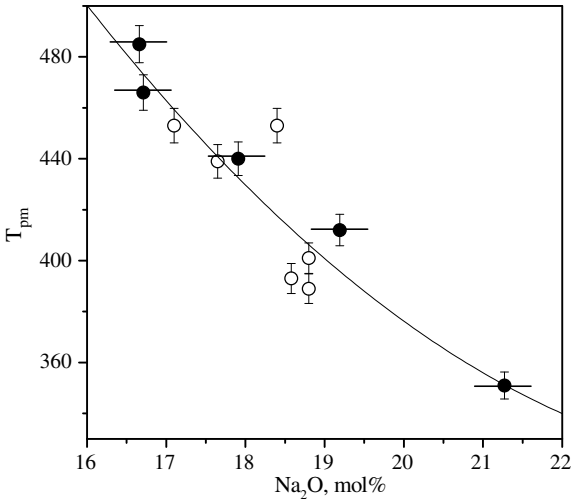

Fig. 3. Temperature of reversible polymorphic transition in fully crystallized glasses taken from DSC hitting curves versus sodium oxide content in the parent glasses. Solid and opened circles refer to analyzed and nominal sodium contents, respectively. The line is placed just to guide the eyes.

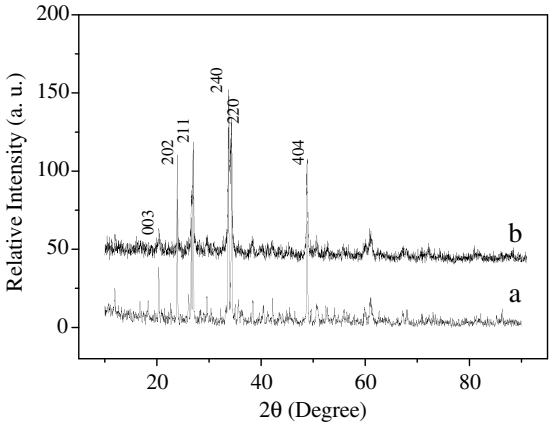

Fig. 5. XRD patterns of TGC1 (a) and TGC2 (b) with about 97% crystallinity – solid solutions with hexagonal structure $N_1C_2S_3$. Crystals have cubic (a) and spherical (b) morphologies. XRD spectrums are close to JCPDS (card 22-1455) for sodium calcium silicate $Na_2Ca_2Si_3O_9$.

of sodium calcium silicate $Na_2Ca_2Si_3O_9$ (JCPDS card 22-1455) [23].

Crystal morphology is one of the factors which affect the transparency of crystallized glasses. Fig. 6 shows examples of a typical transmission spectrum and micrographs of some TGCs with spherical and cubic shaped crystals. The volume fraction crystallized is close to 1.0 in both cases. It is clear that the cubic form favors the transparency of our TGC.

The transmittance of our TGC strongly depends on the degree of crystallinity. Fig. 7 shows a typical plot of transmittance versus volume fraction crystallized together with the reduced specific area of the crystal/glass interface estimated via the following equation [27]:

$$S_R = 2N_L/S_V^{max}, \quad (7)$$

where N_L is the average number of intersections of an arbitrary secant at the crystal/glass interface per unit length and S_V^{max} is maximal value of S_V.

The parameter P_1, which takes into account reflection losses, was estimated in the way described in Section 4. P_1 slightly decreases with crystallized volume fraction (Fig. 8(a)) owing to the increase of the effective refractive index of TGC (Fig. 8(b)). Calculation of P_1 via Eq. (1) with experimental values of refractive index, denoted by stars in Fig. 8(a), corroborates the direct measurements of P_1.

The variation of P_1 is very small (0.915–0.907) as compared with changes of the parameter $P_2 = (\beta + S)$, which characterizes absorption and scattering – and is shown in Fig. 9 as a function of α. According to Fig. 9, the lowest values of P_2 correspond to volume fractions crystallized $\alpha \sim 0.90$–0.96. The transmittance in this α interval varies from 86% to 83% for a 1mm thick plate sample.

For samples containing about 97% crystallized fraction the measured Abbe number is 52.6. Ref. [28] reports a study of mechanical properties of these TGC.

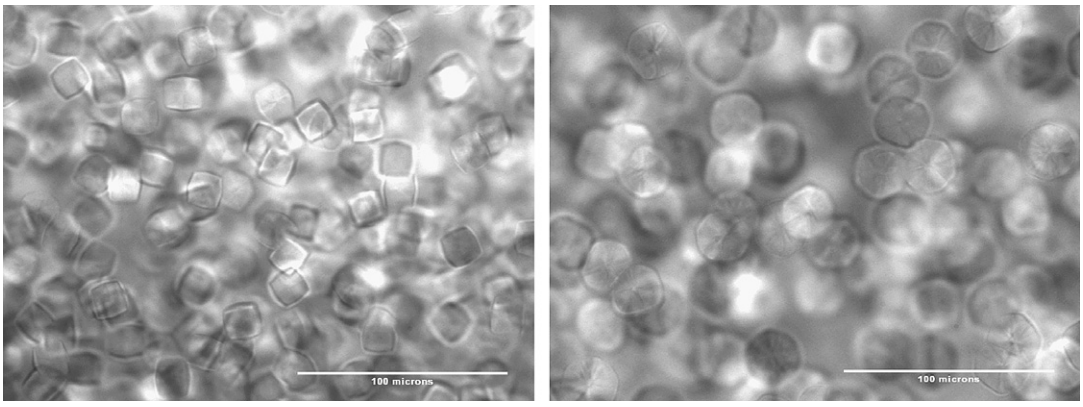

Fig. 4. Optical micrographs of the typical crystal morphologies in glasses having a deficit (left) and an excess (right) of silica relative to the metasilicate composition. Scale bars denote 100 μm.

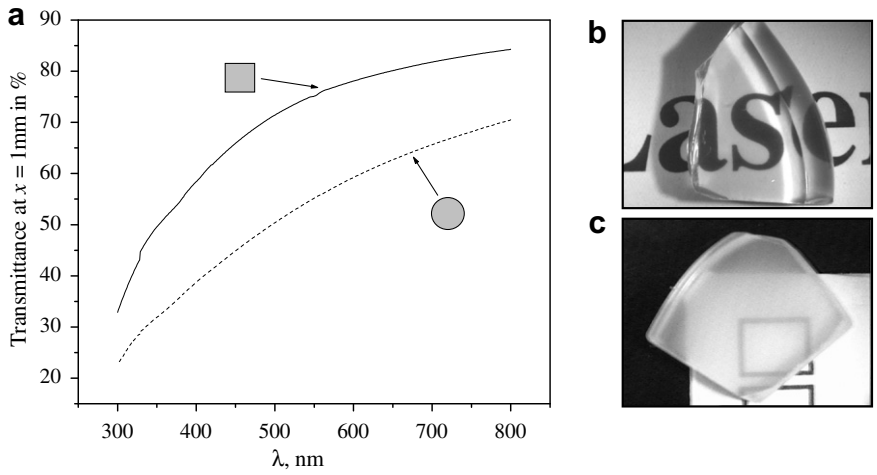

Fig. 6. Transmittance spectra of TGCs with different crystal shapes (a). Optical micrographs of TGC with cubic (TGC-0) (b) and spherical (TGC-2) (c) crystals. The sample thickness is 4 mm (b) and 2 mm (c). The volume fraction crystallized is close to unity in both cases.

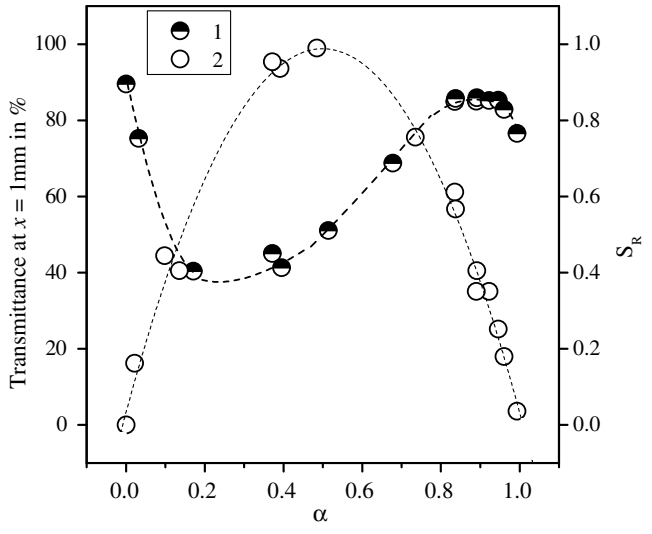

Fig. 7. Transmittance at $\lambda = 800$ nm (1), and reduced specific area of the crystal/glass interface S_R (2) versus volume fraction crystallized for TGC-0.

6. Discussion

In contrast to most of the traditional TGCs, which are based on nano-crystallization, the distinguishing features of the new TGCs above described are their very high degree of crystallinity and micrometric crystal sizes. To understand why such high crystallinity combined with relatively large crystal sizes do not lead to a significant loss of transmittance we must consider the details of the nucleation-growth process in the parent glasses.

As we already mentioned in Section 4, the compositions of the present glasses are close to the metasilicate join $N_1C_2S_3$–$N_1C_1S_2$, which leads to the formation of solid solutions (s/s) [21] with a continuous compositional variation during crystallization [29]. The densities and corresponding refractive indexes of crystals and glasses belonging to this join do not strongly differ. Indeed, the difference between the refractive indexes of $N_1C_2S_3$ crystal and glass of respective stoichiometric composition is only 0.015. Another interesting factor is that the optical birefringence of 1-2-3 crystals is also very low. These similarities favor a low light scattering.

Another feature of these glasses is very important for TGC formation. As we have shown in a previous publication [30], the compositions of the critical nuclei in glasses belonging to the $N_1C_2S_3$–$N_1C_1S_2$ interval are close to $N_1C_2S_3$ and hence they are enriched in sodium as compared with the parent glasses. The reasons for this compositional deviation, discussed in detail in ref. [30], is the decrease in the thermodynamic barrier for nucleation caused by the possible reduction of the interfacial energy due to the increase of sodium in critical nuclei. This scenario agrees with Ostwald's rule of stages, generalized in Ref. [31] for nucleation as '*In phase transformation processes the structure and properties of the critical nucleus may differ qualitatively from the properties both of the ambient and of the newly evolving macrophases. Those classes of critical clusters determine the transformation process, which correspond to a minimum work of critical cluster formation – as compared with all other possible alternative structures and compositions, which may be formed at the given thermodynamic constraints*'. Another interpretation for the precipitation of crystals containing more sodium than the s/s corresponding to the equilibrium phase diagram in deeply undercooled liquids (which are highly viscous) was proposed in Ref. [32]. Those authors connected this compositional deviation from stoichiometry with the high diffusivity of sodium, which exceeds that of calcium by about two orders of magnitude. In any case, for the considered problem it is important that nuclei enriched in sodium continuously grow throughout the phase transformation leading to a depletion of sodium in the glass matrix. This depletion impairs the kinetics of growth and nucleation

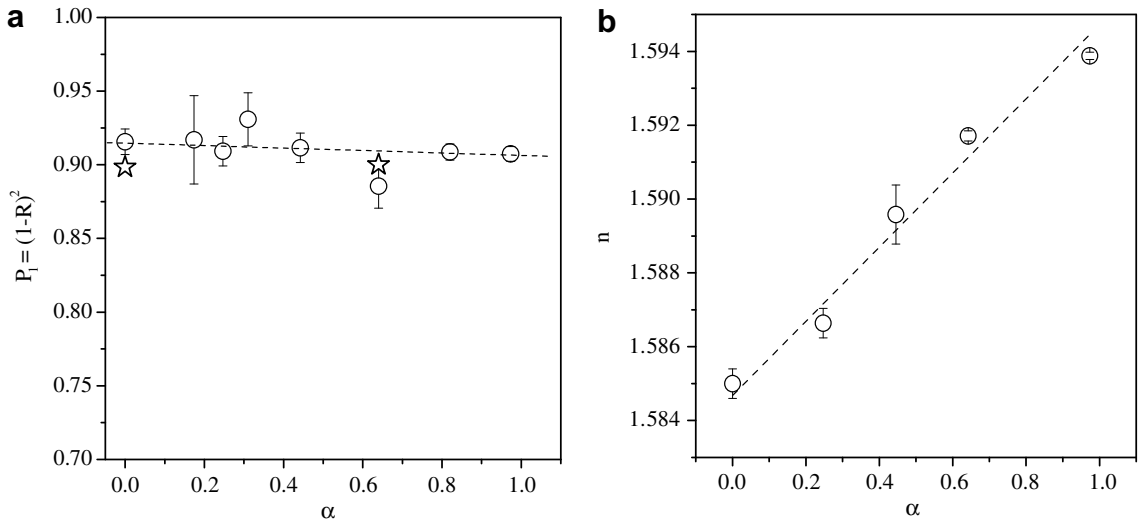

Fig. 8. Value of $P_1 = (1-R)^2$ – light loss due to reflection (a), and refractive index (b) versus volume fraction crystallized. The stars denote P_1 calculated via Eq. (1) using the experimental value of n. The dashed line refers to linear approximations of experimental data.

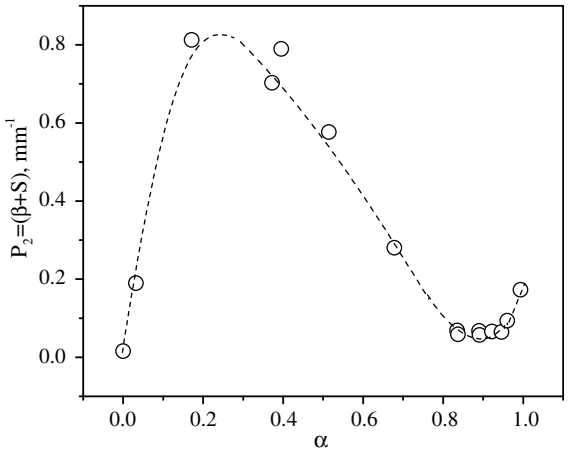

Fig. 9. Absorption and scattering coefficient ($\beta + S$) of TGC-0 versus volume fraction crystallized.

up to the termination of the latter. During phase transformation the average crystal composition approaches that of the parent glass. Therefore, in the advanced stages of crystallization the vitreous matrix (occupying a very small volume fraction) has much less sodium than the crystals.

Such complex crystallization pathway was corroborated by an analysis of the overall crystallization kinetics with the JMAK equation:

$$\alpha(t) = 1 - \exp\{-Bt^{n_A}\}, \tag{8}$$

where α is the volume fraction transformed, n_A is the Avrami coefficient, and B is a parameter that includes the number of crystals (or the crystal nucleation rate) and their growth rate [33]. The Avrami coefficient can be approximately written as

$$n_A = k + 3m, \tag{9}$$

where k and m are taken from the formulas $N \sim t^k$ and $a \sim t^m$ describing the variation of the crystal number (N) and size (a) with time.

Fig. 10(a) and (c) show the volume fraction of crystals and the size of the largest crystals as a function of heat treatment time at $T = 628$ °C for a glass of composition TGC-0 (see Table 1). To estimate the values of n_A and m the data of Fig. 10(a) and (c) were reploted in Avrami (Fig. 10(b)) and logarithmic (Fig. 10(d)) coordinates, respectively. Beginning from approximately 90–110 min the phase transformation occurs solely due to crystal growth, since $n_A \cong 3m$ and $k \cong 0$ (according to Eq. (9)).

The evolution of the glass matrix and crystal compositions during phase transformation was corroborated by direct EDS measurements, whose results for the same TGC are shown in Fig. 11. According to these data, the sodium content in the crystalline phase is always higher than that in the corresponding glassy matrix. This compositional difference is one of the main reasons for the improved transparency of the present TGC. Analyzing the data of Fig. 11 together with the compositional dependencies of the refractive indexes of glass and crystal (s/s), shown in Fig. 12(a), one realizes that sodium enrichment of the crystalline phase relatively to that of the parent glass approximates the refractive indexes of crystal and glassy phase. Knowing the compositional variations of the glassy matrix and the crystals, and the functions $n(C_{Na_2O})$ for both crystal and glass, one can estimate the evolution of refractive indexes during glass crystallization. An example of such evolution is shown in Fig. 12(b). The solid and dashed lines refer to the crystal and the glassy matrix. The top and bottom horizontal lines show the refractive indexes for parent glass and fully crystallized sample, respectively.

Indeed, the difference between the refractive indexes of the crystalline and glassy phase is about four times lower than that if the crystal and glassy matrix compositions were

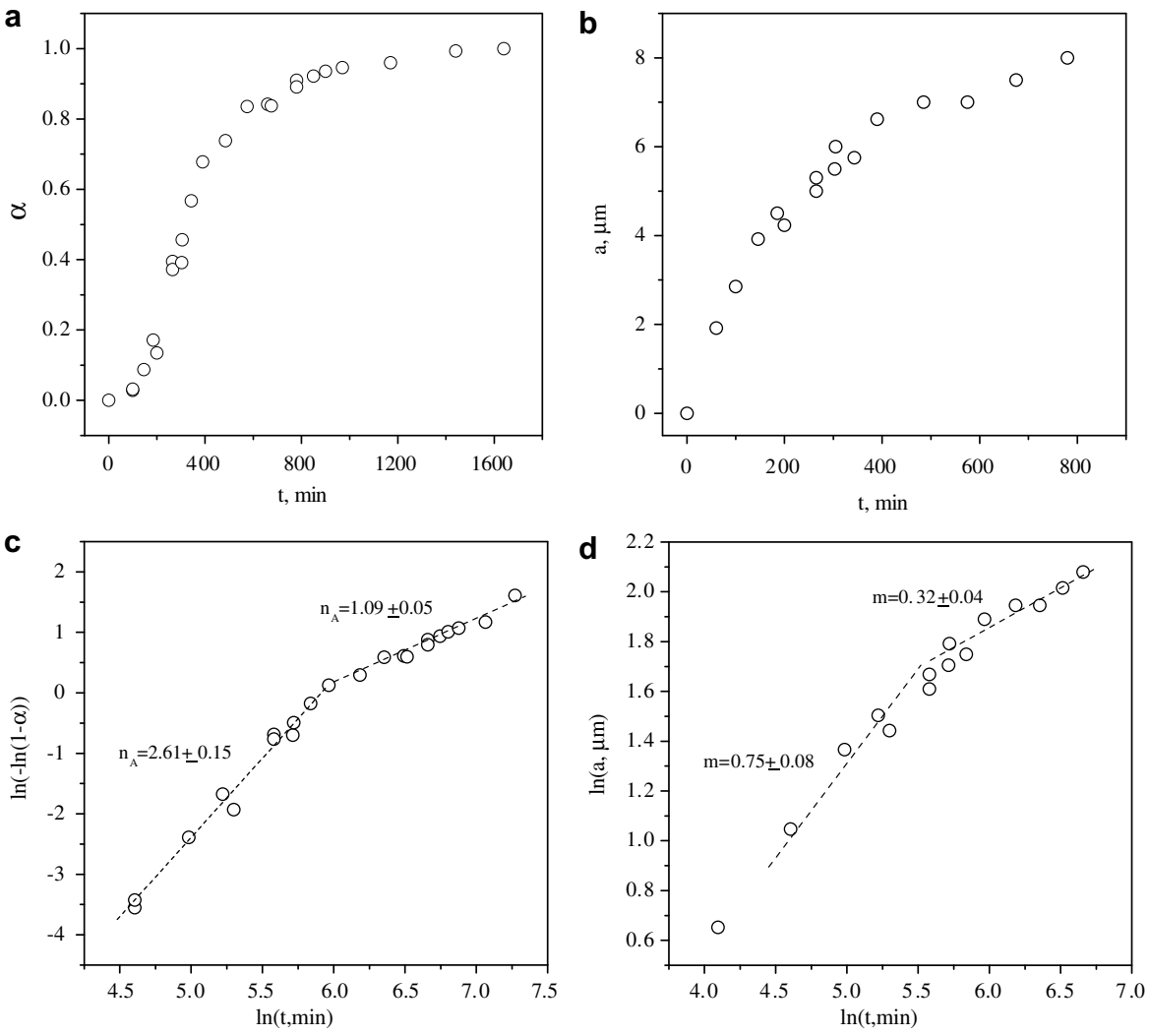

Fig. 10. Volume fraction of crystals (a, c) and size of the largest crystals (b, d) in TGC-0 versus time of heat treatment at 628 °C. The dashed lines refer to linear approximations.

equal. Moreover there is a (slight) further reduction of this difference with increasing degree of crystallinity. This phenomenon results in a significant decrease of *the refractive index dependent term*, $\left[\frac{M^2-1}{M^2+2}\right]^2$, which provides a good description of the scattered light intensity also in the case of large particles. Fig. 13 shows $\left[\frac{M^2-1}{M^2+2}\right]^2$ for different volume fractions crystallized.

Thus, a TGC with about 95–97% crystallinity consists of relative large crystals having a composition very close to that of the (initial) parent glass, and thin areas of glassy phase with a composition close to the stoichiometric $N_1C_2S_3$ (for TGC-0 and TGC-1). In other words, the residual glassy phase is depleted in sodium as compared with the crystalline phase. Here it should be noted that we are dealing with average compositions. Possible compositional gradients are expected, especially within crystals, and noticeably complicate this picture.

In addition to the similarity of the refractive index of the crystals and surrounding glassy matrix, the scattering coefficient, S, is affected by the average crystal size. Therefore, the thermal history leading to crystallization is of great importance. Fig. 14 shows the transmission spectra of partly crystallized glasses (~42% crystallinity) caused by single and double heat-treatments.

According to Eq. (3) the increased transmittance shown in curves 1, 2 result from an increased average crystal size from 7.5 to 47 μm at a fixed crystallized volume fraction. This crystal size increase also weakens the $I(\lambda)$ dependence (see Section 3). Indeed, one can observe that the transmission curve 2 in Fig. 14 is flatter than curve 1, which is related to smaller crystal sizes.

The scattering theory deals with isolated particles in a surrounding medium. In the early and middle stages of phase transformation isolated crystals indeed represent such particles. Their total volume and size increases during crystallization. In the advanced stages of crystallization isolated areas of glass embedded within the crystalline phase act as scattering particles whose volume and size decreases during crystallization. This evolution is

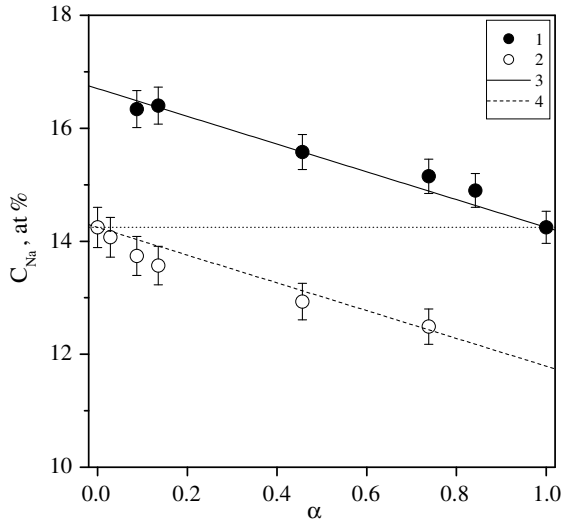

Fig. 11. Average sodium content in the crystalline phase (1) and glassy matrix (2) versus volume fraction crystallized of TGC-0. The solid line (3) is a linear fit to experimental data. The dashed line (4) was calculated from the crystal and parent glass compositions. The dotted line shows the sodium content in the parent glass and in the fully crystallized sample.

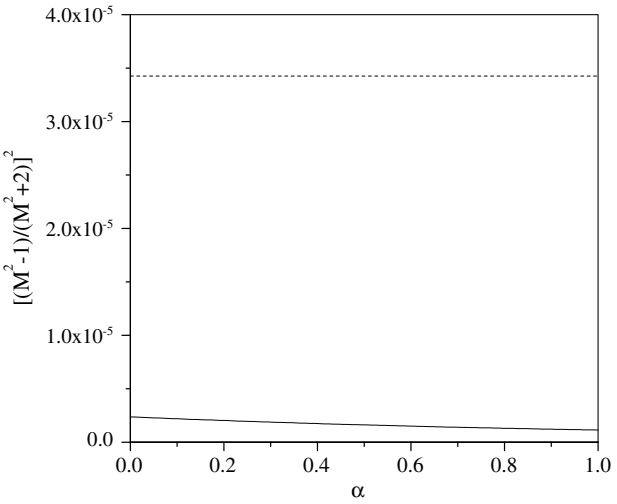

Fig. 13. Parameter $\left[\frac{M^2-1}{M^2+2}\right]^2$ that gives the scattering due to the difference between the reflective indexes of crystals and glass matrix versus volume fraction crystallized. The dotted line refers to crystals and glassy matrix having same composition.

reflected by the dependence of specific interface area, which reveals a maximum (see Fig. 7, curve 2). Since the scattering coefficient depends on the volume and size of the particles, the 'switch' of the microstructure (from crystals in a glassy matrix to glassy 'lakes' in a crystalline matrix) results in the minimum of the curve of TGC transmittance versus volume fraction crystallized (Fig. 7, curve 1).

To summarize, the TGC transmittance is affected by the continuous compositional changes of both glassy matrix and crystalline phase. Crystallization leads to an approximation of the refractive indexes of the crystalline and glassy phases. Such changes determine the TGC transmittance, and this could be one of the reasons why the position of the minimum on curve 1 does not coincide with that of the maximum on curve 2. It should be also noted that before impingement the crystals have more or less isometric shape, while the shapes of the glassy 'lakes' in a crystalline matrix at advanced and final stages of phase transformation are more complex. A decrease of transmittance in the very final stage (for crystallinities higher than about

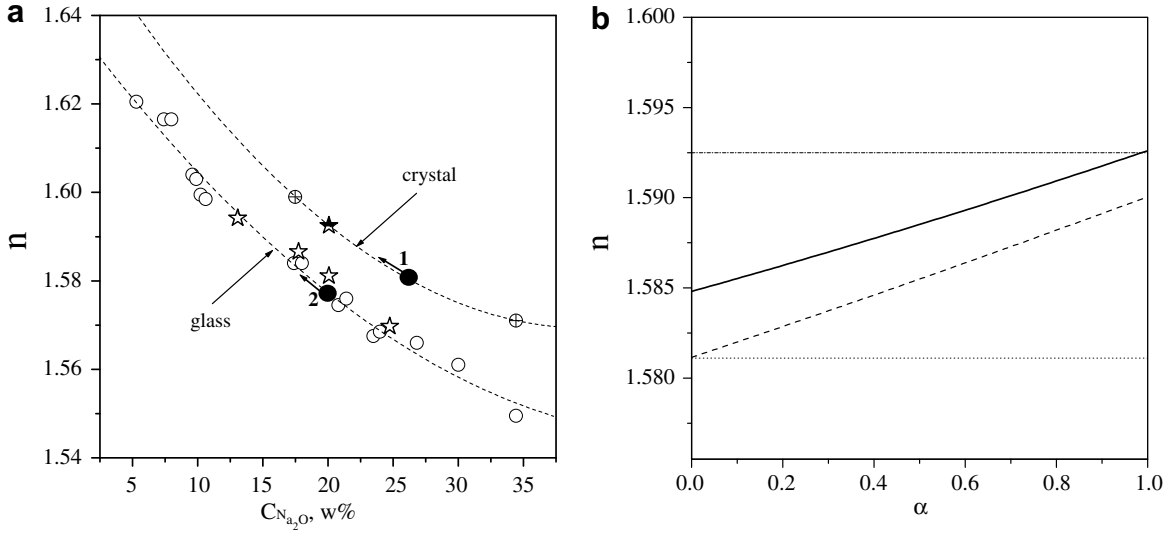

Fig. 12. (a) Refractive indexes of crystal and glass versus of sodium oxide content. Stars refer to our TGC. Open circles refer to data taken from Ref. [34]. Dashed lines resulted from a polynomial fit to the experimental data. Black points 1 and 2 correspond to the critical nucleus composition and composition of the parent glass, respectively. The arrows show the direction of the composition evolution during phase transformation. (b) Evolution of refractive indexes of crystals (solid line) and glassy matrix (dashed line) versus volume fraction crystallized. Dotted and dashed-dotted lines show the refractive indexes of the parent glass ($\alpha = 0$) and fully crystallized sample ($\alpha = 1$).

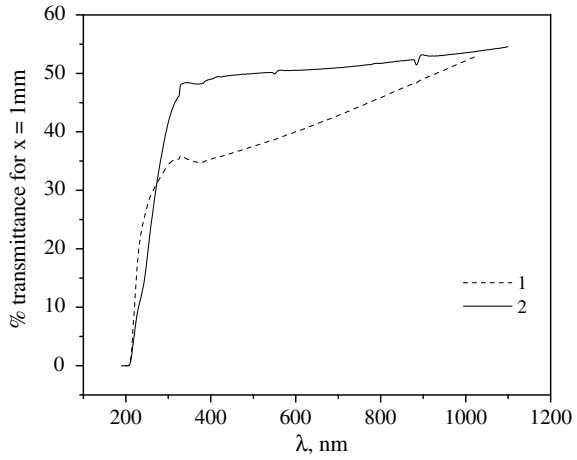

Fig. 14. Transmission spectra of partly crystallized glass of composition TGC-2 containing about 42% crystal phase by single (2) and double (1) heat treatments, having crystal number densities about $1.2.10^4$ and $2{\cdot}10^6$ mm^{-3} and crystal diameters of 47 and 7.5 μm, respectively.

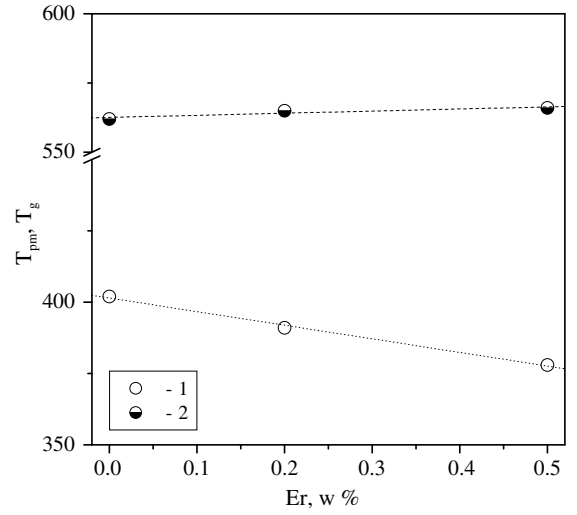

Fig. 15. Temperature of reversible polymorphic phase transition (1) and glass transition temperature (2) versus Er content.

97%) is caused by the appearance of spontaneous micro cracks in these TGC, since the blockaded glassy areas are exposed to high stresses [35].

As we already mentioned, the crystals in our TGCs are $Na_{4+2x}Ca_{4-x}[Si_6O_{18}]$ s/s which are based on the hexagonal structure of sodium calcium silicate $Na_4Ca_4[Si_6O_{18}]$. This structure has cation sites only partly occupied by Na and Ca ions [22]. Thus we expect that transition metals or rare-earth elements could be inserted as substitutional sites in these structures. Fig. 15 shows that, indeed, first attempts to introduce Er in our TGC resulted in a pronounced increase in the reversible isomorphous phase transition temperatures T_{pm} of the s/s crystals. This result can be interpreted as an evidence for Er insertion in s/s.

The Abbe number of our TGC is similar to that of commercial soda-lime–silica glass and is surprising for a material containing 97% crystallized fraction. Just for comparison purposes, the Abbe number of the human eye is approximately 45, and thus any lens with smaller Abbe number can compromise the vision quality. This Abbe number, 52.6, indicates that our TGC does not suffer strong light dispersion.

7. Conclusions

As opposed to the typical traditional transparent glass–ceramics, which have nano-size crystals and low to moderate crystallinity, we developed a new type of TGC having large (micrometric) grain size and high crystallized volume fraction. Their high transmittance mainly results from simultaneous variations of the glass-matrix and s/s-crystal compositions during crystallization, which lead to a considerable decrease in the difference between the respective refractive indexes of the two phases. Therefore the difference between the respective refractive indexes prevails regardless of crystal size when the aim is to improve transmittance. Preliminary tests indicate that this new family of TGC can be further developed by doping them with transition metal and rare-earth elements and perhaps be used as optical components.

Acknowledgments

We are indebted to Fapesp – The São Paulo State Research Foundation (Brazil) for funding this research, and to CAPES (Brazil) for a doctoral grant to TB.

References

[1] P.W. Mcmillan, Glass–Ceramics, Harcourt Publishers Ltd., 1979.
[2] G.H. Bell, L.R. Pinckney, J. Am. Ceram. Soc. 82 (1999) 5.
[3] G.H. Beall, D.A. Duke, J. Mater. Sci. 4 (1969) 340.
[4] Patents, e.g.: WO200290279-A; WO200290279-A1; US2003013593-A1; US6632758; EP1170262-A; EP1170262-A1; US2002022564-A1; CN1333194-A; JP2002154841-A; KR2002003502-A.
[5] W. Holland, G. Beall, Glass–Ceramic Technology, The American Ceramic Society, 2002.
[6] A.S. Gouveia-Neto, E.B. da Costa, L.A. Bueno, S.J.L. Ribeiro, J. Alloys Compd. 375 (2004) 224.
[7] X. Duan, D. Yuan, C. Luan, Z. Sun, D. Xu, M. Lu, J. Non-Cryst. Solids 328 (2003) 228.
[8] X. Zhang, M.A. Hongli, J. Lucas, J. Non-Cryst. Solids 337 (2004) 130.
[9] M. Mortier, A. Monteville, G. Patriarche, G. Mazé, F. Auzel, Opt. Mater. 16 (2001) 255.
[10] A.S. Gouveia-Neto, E.B. Da Costa, L.A. Bueno, S.J.L. Ribeiro, J. Lumin. 110 (2004) 78.
[11] T. Suzuki, G.S. Murugan, Y. Ohishi, Appl. Phys. Lett. 86 (2005).
[12] M. Clara Gonçalvez, L.F. Santos, R.M. Almeida, C. R. Chim. 5 (2002) 845.
[13] L.L. Kukkonen, I.M. Reaney, D. Furniss, M.G. Pellatt, A.B. Seddon, J. Non-Cryst. Solids 290 (2001) 25.
[14] S. Todoroki, S. Inoue, Appl. Surf. Sci. 223 (2004) 39.
[15] W. Pannhorst, Glass Tech. 45 (2004) 51.
[16] L.R. Pinckney, J. Non-Cryst. Solids 255 (1999) 171.
[17] R. Tilley, Colour and the Optical Properties of Materials, John Wiley, 1999, p. 335.
[18] S. Hendy, Appl. Phys. Lett. 81 (2002).

[19] W.D. Kingery, H.K. Bowen, D.R. Uhlmann, Introduction to Ceramics, 2nd Ed., Wiley, New York/London/Sydney/Toronto, 1976.
[20] H. Rawson, Properties and Applications of Glass, Elsevier Science, 1980.
[21] G.K. Moir, F.P. Glasser, Phys. Chem. Glasses 15 (1974) 6.
[22] H. Ohsato, Y. Takeuchi, I. Maki, Acta Crystallogr. B 46 (1990) 125.
[23] E.N. Soboleva, N.S. Yuritsin, V.L. Ugolkov, Glass Phys. Chem. 30 (2004) 481.
[24] I. Maki, T. Sugimura, J. Ceram. Assoc. Jpn. 76 (1968) 144.
[25] V.M. Fokin, E.D. Zanotto, J. Non-Cryst. Solids 353 (2007) 2459..
[26] C.J.R. Gonzalez-Oliver, PhD thesis, The University of Sheffield, 1979, p. 175.
[27] R.T. DeHoff, Quantitative Microscopy, McGraw-Hill Book Company, 1968.
[28] T. Berthier da Cunha, J.P. Wu, O. Peitl, V.M. Fokin, E.D. Zanotto, L. Inannucci, A.R. Boccaccini, Adv. Eng. Mater. 9 (2007) 119.
[29] V.M. Fokin, O.V. Potapov, E.D. Zanotto, F.M. Spiandorello, V.L. Ugolkov, B.Z. Pevzner, J. Non-Cryst. Solids 331 (2003) 240.
[30] V.M. Fokin, E.D. Zanotto, N.S. Yuritsyn, W.P. Schmelzer, J. Non-Cryst. Solids 352 (2006) 2681.
[31] J.W.P. Schmelzer, J. Gutzow, J. Schmelzer Jr., J. Chem. Phys. 112 (2000) 3820.
[32] M. Roskosz, M.J. Toplis, P. Besson, P. Richet, J. Non-Cryst. Solids 351 (2005) 1266.
[33] I. Gutzow, J. Schmelzer, The Vitreous State: Thermodynamics, Structure, Rheology and Crystallization, Springer, Berlin, 1995.
[34] SCi Glass 6.5 http://www.esw.software.com/sciglass.
[35] V.R. Mastelaro, E.D. Zanotto, J. Non-Cryst. Solids 194 (1996) 297.